

Capturing Choline–Aromatics Cation– π Interactions in the MARTINI Force Field

Hanif M. Khan,* Paulo C. T. Souza, Sebastian Thallmair, Jonathan Barnoud, Alex H. de Vries, Siewert J. Marrink, and Nathalie Reuter*

Cite This: *J. Chem. Theory Comput.* 2020, 16, 2550–2560

Read Online

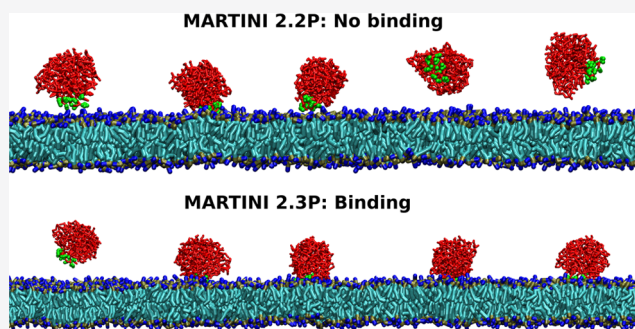
ACCESS |

Metrics & More

Article Recommendations

Supporting Information

ABSTRACT: Cation– π interactions play an important role in biomolecular recognition, including interactions between membrane phosphatidylcholine lipids and aromatic amino acids of peripheral proteins. While molecular mechanics coarse grain (CG) force fields are particularly well suited to simulate membrane proteins in general, they are not parameterized to explicitly reproduce cation– π interactions. We here propose a modification of the polarizable MARTINI coarse grain (CG) model enabling it to model membrane binding events of peripheral proteins whose aromatic amino acid interactions with choline headgroups are crucial for their membrane binding. For this purpose, we first collected and curated a dataset of eight peripheral proteins from different families. We find that the MARTINI CG model expectedly underestimates aromatics–choline interactions and is unable to reproduce membrane binding of the peripheral proteins in our dataset. Adjustments of the relevant interactions in the polarizable MARTINI force field yield significant improvements in the observed binding events. The orientation of each membrane-bound protein is comparable to reference data from all-atom simulations and experimental binding data. We also use negative controls to ensure that choline–aromatics interactions are not overestimated. We finally check that membrane properties, transmembrane proteins, and membrane translocation potential of mean force (PMF) of aromatic amino acid side-chain analogues are not affected by the new parameter set. This new version “MARTINI 2.3P” is a significant improvement over its predecessors and is suitable for modeling membrane proteins including peripheral membrane binding of peptides and proteins.



1. INTRODUCTION

Coarse grain (CG) molecular dynamics (MD) simulations have become increasingly popular in recent years for the modeling of complex and large biomolecular systems.¹ By reducing the system complexity these models allow for large gains in computing time and CG MD simulations can probe longer timescales than conventional all-atom simulations. One of the currently most used CG models is MARTINI,² which has parameters available for major biomolecules (lipids,^{3,4} proteins,^{5,6} carbohydrates,⁷ and nucleic acids^{8,9}). The MARTINI model has been widely used to study lipid–protein interactions, in particular, involving transmembrane proteins,^{10,11} but comparatively fewer studies of peripheral membrane protein binding have been performed.^{12–17}

The binding of peripheral proteins to membranes is modulated by reversible and transient interactions with the membrane surface.¹⁸ Binding typically proceeds through the interaction of an electropositive region of the protein surface with the negatively charged lipids (e.g., phosphatidylinositol (PI), phosphatidylinositol monophosphate (PIP), phosphatidic acid (PA), phosphatidylserine (PS), phosphatidylglycerol (PG)) followed by the partitioning of hydrophobic amino

acids in the bilayer core and at the interface.^{18,19} The three aromatic amino acids tryptophan, tyrosine, and phenylalanine are often found partitioning at the interface, while aliphatic ones, such as isoleucine or leucine, tend to insert deeper.²⁰ Interestingly, an increasing number of interfacial aromatics are being observed engaging in cation– π interactions with the positively charged headgroups of phosphatidylcholine (PC) lipids not only for peripheral^{21–27} but also for transmembrane²⁸ proteins.

Accurate modeling of peripheral protein membrane binding by CG simulations requires that these interactions are accounted for in the force field. Unlike charge–charge interactions and partitioning behavior that are fairly well described, cation– π interaction remains a challenge for additive force fields. Recently, we proposed and evaluated a

Received: November 29, 2019

Published: February 25, 2020



Table 1. Peripheral Proteins Tested and CG Simulation Details^f

protein	PDB id	bilayer composition	test type	force field	starting configuration	simulation length (ns)	no. of simulations	total time (ns)
BtPI-PLC	3EA1/ 2OR2	DMPC	MBT ^a	2.2P	MBO ^c	500	5	2500
			MDT ^b	2.2P	MBS ^d	500	5	2500
			MBT	2.3P	MBO	500	5	2500
			MBT	2.3P	RO ^e	1000	5	5000
PH domain (PLC- δ 1)	1MAI	POPC/POPS/PIP ₂ /PIP ₃ (73:20:5:2)	MBT	2.2P	RO	1000	1	1000
			MBT	2.3P	RO	1000	1	1000
PR3	1FUJ	POPC	MBT	2.2P	MBO	1000	1	1000
			MBT	2.3P	MBO	1000	1	1000
Equinatoxin	1IAZ	POPC	MBT	2.2P	MBO	500	1	500
			MBT	2.3P	MBO	500	1	500
PLA ₂	1POA	DMPC	MBT	2.2P	RO	1000	1	1000
			MBT	2.3P	RO	1000	1	1000
PC-specific SaPI-PLC	4I8Y	POPC	MBT	2.2P	RO	1000	1	1000
			MBT	2.3P	RO	1000	1	1000
WT SaPI-PLC	4F2T	POPC	MBT	2.3P	RO	500	2	1000
GLTP	1WBE	POPC	MBT	2.2P	RO	400 + 362	2	762
			MBT	2.3P	RO and MBO	500	2	1000

^aMBT: membrane binding test. ^bMDT: membrane detachment test. ^cMBO: membrane-binding orientation. ^dMBS: membrane-bound structure. ^eRO: randomized orientation. ^fTests with other interaction levels are reported in Table S1 and are not included here.

simple modification of the CHARMM36 force field to improve its treatment of choline–aromatics cation– π interactions.^{29,30} This followed a careful evaluation of the performance of the atomistic force field to reproduce the energetics and structure of cation– π interactions of relevant model systems and in simulations of peripheral proteins. No such evaluation has been carried out for CG models yet, although the SIRAH force field reported that cation– π interactions have been incorporated in their phospholipid models.³¹ Simulations of peripheral proteins have been reported in recent years, and interestingly, most of these proteins mediate membrane interactions primarily driven by electrostatic interactions³² such as the recognition of phosphatidylinositides-containing membranes by pleckstrin homology (PH) domains.^{12–14,33,34} Several works have also tested the performance of the MARTINI CG model at modeling hydrophobic partitioning of lipidated proteins,^{35,36} but no examples where cation– π interactions act as major contributors have been evaluated yet.

In this work, we test the ability of the currently most accurate version of the MARTINI force field (the polarizable version 2.2P) to model the peripheral binding of proteins whose membrane binding depends on choline–aromatics cation– π interactions and on insertion of aromatic amino acids at the bilayer interface. For this, we choose the *Bacillus thuringiensis* phosphatidylinositol-specific phospholipase C (BtPI-PLC) because the mechanism by which it binds membranes is well-characterized both computationally and experimentally.^{21,25} We show that simulations with the polarizable MARTINI CG model do not capture binding events and suggest modifications of the interaction matrix to improve this. This modified matrix is validated on a dataset of eight peripheral proteins, including negative controls. We also verify that the modified matrix does not introduce biases in simulations of bilayers, transmembrane proteins, and control peripheral proteins not relying on interfacial aromatics to bind PC-rich bilayers. Our work shows that the proposed force field, coined version 2.3P, can improve the description of the role of

interfacial aromatics in peripheral protein binding to membranes, including those reliant on choline–aromatics cation– π interactions.

2. MATERIALS AND METHODS

2.1. Simulations of Peripheral Proteins. We ran simulations of eight peripheral proteins and of their binding to lipid bilayers of various compositions. The proteins are listed in Table 1 along with their PDB IDs, the bilayer compositions, and starting configurations used. All were simulated with both the polarizable MARTINI 2.2P force field and the modified version (2.3P). The number of simulations run and their lengths are also given in Table 1.

2.1.1. System Preparation and Simulations. The protein structures were obtained from PDB except for BtPI-PLC for which no structure of the wild type has been solved. We used a model built by Grauffel et al.²¹ from the Y247S/Y251S mutant structure of BtPI-PLC (PDB id: 3EA1).³⁷ The missing tyrosine side chains were taken from the W47A/W242A mutant structure of BtPI-PLC (PDB id: 2OR2).³⁸ The structure was then carefully minimized using backbone (BB) and side-chain restraints.²¹ All proteins structures were processed and prepared for coarse grain simulations using martinize.py script.⁶

The protein–membrane complexes were prepared using the insane tool.³⁹ The proteins were placed above the bilayer either in their membrane binding orientation (MBO) or in a randomized orientation (RO) (Figure 1A,C). The bound mode (MBS) is obtained by manually docking the protein in the membrane binding orientation (Figure 1B). The membrane binding orientations were either obtained from the literature (all-atom simulations) or taken from the orientation of proteins in membranes (OPM) database.⁴⁰ The distance between the centers of mass of the protein and the membrane was set to be between 6 and 7 nm depending on the protein size and shape. For each protein, we ran multiple independent simulations differing by the protein–

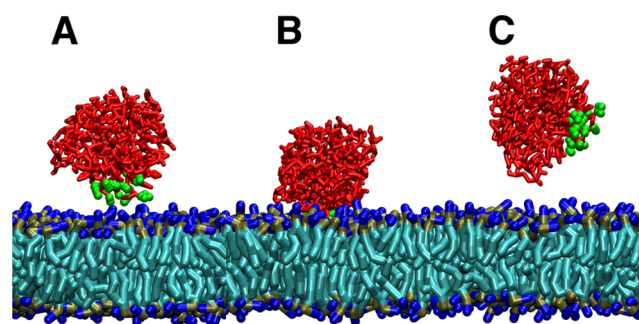


Figure 1. Starting orientations used for membrane binding (A, C) and membrane detachment (B) simulations of peripheral proteins, illustrated with *BtPI-PLC* (red licorice and green van der Waals (VDW) spheres). Membrane binding simulations were performed starting from either the known membrane-binding orientation with the interfacial binding site (green VDW spheres) facing the bilayer (A) or a random orientation (C) to overcome the potential bias due to the choice of the starting configuration. Membrane detachment simulations were carried out starting from known membrane-bound structures. For clarity, waters and ions are not shown.

membrane distance (increment of 0.1 nm) and in some cases by the protein orientation that was randomized. The systems were placed in a box of $8.96 \times 8.96 \times 16 \text{ nm}^3$, which resulted in bilayers with 288 lipids for the single-component bilayers: 144 1-palmitoyl-2-oleoyl-phosphatidylcholine (POPC) or dimyristoyl-phosphatidylcholine (DMPC) in each leaflet. The mixed bilayers, composed of POPC, 1-palmitoyl-2-oleoyl-*sn*-glycero-3-phospho-L-serine (POPS), phosphatidylinositol (4,5)-bisphosphate (PIP₂) and phosphatidylinositol (3,4,5)-trisphosphate (PIP₃) in a 73:20:5:2 molar ratio, contained 284 lipids (142 lipid in each leaflet). The POPC or DMPC bilayer systems were solvated with polarizable water molecules,⁴¹ and the system was neutralized with NaCl counterions. For the mixed bilayer, a salt concentration of 0.15 M NaCl was used together with polarizable water. An elastic network was applied to the proteins in all simulations based on the “Elnedyn” model.⁴²

Each solvated protein–membrane complex was then minimized for 50 000 steps using the steepest descent algorithm. After the minimization, the system was equilibrated for 1 ns and subsequently production simulations were performed (see Table 1), using the leap-frog integrator in the NPT ensemble. The temperature was set to 310 K and maintained using the *v*-rescale thermostat.⁴³ The pressure was set to 1 bar and maintained using the Parrinello–Rahman barostat.⁴⁴ Semi-isotropic pressure coupling was applied for these systems. For the calculation of nonbonded interactions, a pair list was generated using the Verlet scheme with a buffer tolerance of 0.005. The Coulombic terms were calculated using particle mesh Ewald⁴⁵ (PME) and a real-space cutoff of 1.1 nm. The relative dielectric constant was set to 2.5, as recommended for the polarizable MARTINI model. For the VDW terms, we used a cutoff scheme with a cutoff value of 1.1 nm and the Verlet cutoff scheme for the potential-shift.⁴⁶ All simulations were carried out using GROMACS (v. 2016.x).⁴⁷ The time step used for these simulations was 20 fs except for the cases where numerical instability was observed, in which case the time step was reduced to 10 fs.

2.1.2. Simulation Analyses. To quantify the depth of insertion in the lipid bilayer for individual residues, we calculated the distance along the membrane normal *z* between

the center of mass of the residue and the average phosphate plane of the binding leaflet. A negative value means that the residue is inserted below the phosphate plane. The calculation of the depth of insertion was done after membrane binding of the proteins that underwent successful binding events. In cases where the protein would not bind to the bilayer, the analysis was done throughout the trajectory.

To identify binding events and characterize them, we also calculated the minimum distance between proteins and bilayers using the *gmx mindist* tool. However, the minimum distance alone does not distinguish between different binding orientations of the protein and can be misleading. This is equally true for density profiles. Hence, we also calculated the tilt angle of the protein with respect to the membrane normal. For *BtPI-PLC*, we used the known membrane bound orientation as a reference and a vector defined by the backbone bead of the Ile43 (membrane-binding residue) and of Lys150 (located opposite to the binding face of the protein). The motivation was not to find a fixed tilt angle value but rather to see when it reaches a stable value (and fluctuates around that value), which will identify the binding events. Multiple peak values of the tilt angles will identify two or more distinct binding modes, which were further checked to compare the binding mode with experiments or all-atom simulations data from the literature.

2.2. Simulations of Transmembrane Proteins. We performed 500 ns long simulations embedding a rhodopsin (PDB ID: 1U19) monomer in a POPC bilayer with both MARTINI 2.2P and MARTINI 2.3P. The protein was briefly minimized in vacuum with the steepest descent algorithm for 10 steps. Then, the protein was embedded in a POPC bilayer using the *insane* tool in a box of $13.5 \times 13.5 \times 12.7 \text{ nm}^3$, which resulted in a bilayer with 525 POPC lipids (265 POPC in the upper leaflet and 260 in the lower leaflet). The system was then solvated with 12 447 polarizable water molecules and neutralized with NaCl counterions. The resulting solvated system was further minimized with the steepest descent algorithm for 5000 steps and equilibrated for 500 ps before the 500 ns production run, using a 10 fs time step. All other simulation parameters were similar to those used for the peripheral proteins.

The analyses were carried out on the last 490 ns of the production run using GROMACS tools,⁴⁸ with errors estimated by block averaging. We calculated the bead density for water, protein backbone (BB bead), phosphate (PO4 bead), and choline (NC3 bead) groups along the bilayer normal (the *z*-dimension of the simulation box). Protein–lipid contacts were counted using a distance cutoff of 0.7 nm between the beads. Tilt angles were computed between the axis of helix 4 (described by the backbone beads of residues 150–171) and the bilayer normal. The occupancy of POPC heads around rhodopsin was computed by means of the “occupancy” option of the VolMap tool of VMD⁴⁹ with a 0.2 nm resolution grid.

2.3. Lipid Bilayer Systems. We set up and simulated three different lipid bilayer systems of increasing complexity to control that the lipid and bilayer properties remained unaffected by our modification of MARTINI 2.2P. The first and simplest system was a single-component bilayer of 242 dilinoleoyl-phosphatidylcholine (DLiPC) in a box of $8.8 \times 8.8 \times 8.0 \text{ nm}^3$ set up using the *insane* tool.³⁹ It was solvated with 2966 CG polarizable water beads. After a steepest descent minimization of 500 steps, the system was equilibrated for 500

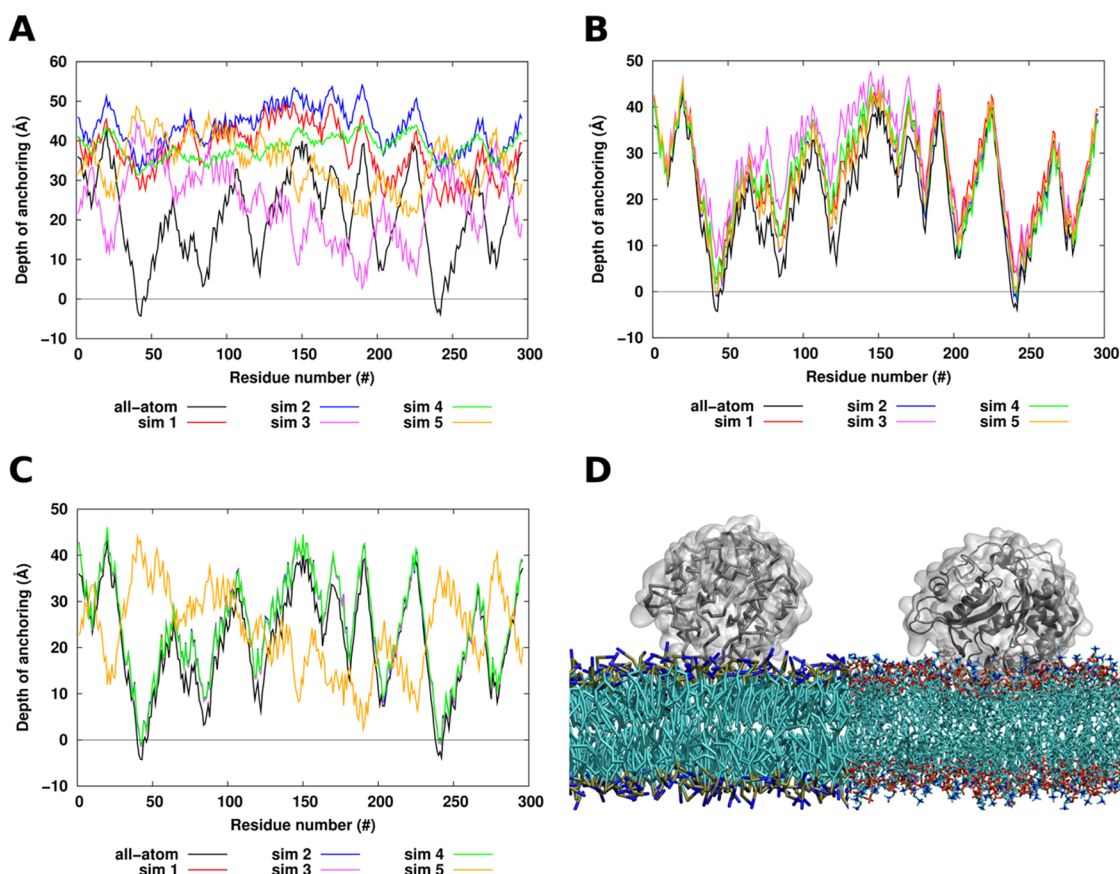


Figure 2. Depth of anchoring of each amino acid in *BtPI-PLC* calculated from simulations with (A) MARTINI 2.2P (MBO), (B) MARTINI 2.3P (MBO), (C) MARTINI 2.3P and using random starting orientations (RO). The reference profile (black) was obtained from all-atom simulations by Grauffel et al.²¹ The average position of the phosphate plane (black line at $y = 0$) is chosen as reference of insertion. In all cases except one, with MARTINI 2.3P (B, C), the protein manages to bind the membrane in the correct orientation. On the other hand, MARTINI 2.2P did not manage to localize the protein in the membrane (A). (D) Membrane binding mode obtained for *BtPI-PLC* using MARTINI 2.3P CG (left), and all-atom (right) simulations. All-atom structure is taken from Grauffel et al.²¹ Note the similarities in both binding modes. For CG snapshot, membrane and the protein backbone (gray) is shown using licorice representation. For the all-atom snapshot, the protein backbone is shown in a cartoon representation. For clarity, waters and ions are not shown, nor are the hydrogen atoms shown. In both cases, proteins are highlighted using transparent QuickSurf representation of VMD.⁴⁹

ps (time step: 10 fs) and 30 ns (time step: 20 fs) at 310 K and 1 bar. The production run of 1 μ s was performed with a time step of 20 fs at 310 K and 1 bar. Other simulation parameters were as described in Section 2.1.

The second system was a mixture of 204 DLiPC and 36 cholesterol (CHOL) molecules at a molar ratio of 85:15. It was solvated with ~ 2000 CG polarizable water beads in a box of $8.8 \times 8.8 \times 8.0$ nm³. A salt concentration of 0.1 M NaCl was added. The minimization, equilibration, and production runs were performed as for the previous system.

The most complex bilayer was set up starting from a phase-separated lipid bilayer consisting of 824 dipalmitoyl-phosphatidylcholine lipids (DPPC), 544 DLiPC, and 576 CHOL molecules and generated earlier with standard MARTINI 2.2.⁵⁰ For the purpose of this work, we exchanged the ~ 31 000 water beads with polarizable water beads. It contained 0.2 M concentration of NaCl. After an equilibration of 1 ns (time step 2 fs), a 2 μ s production run was started using a time step of 20 fs.

For all systems, we analyzed the average area per lipid (APL), area compressibility, tail order parameter, and bilayer thickness. In addition, we calculated the lateral density profile of the second and third systems and evaluated the CHOL flip-

flop rate. In the third system, we also performed a neighbor analysis of the different lipid species.

2.4. Membrane Translocation Potential of Mean Force (PMF) for Amino Acids. We calculated the potential of mean force (PMF) of the side-chain analogues as a function of the distance from their center of mass to the center of mass of a dioleoylphosphocholine (DOPC) bilayer using umbrella sampling simulations and the weighted histogram analysis method (WHAM⁵¹). We carried out a series of simulations with distances from 0.0 to 4.0 nm with a 0.1 nm increment. The distance was restrained with a harmonic potential using a force constant of 1000 kJ/(mol nm²). Each system contained one side-chain analogue, a bilayer of 162 DOPC molecules, and water (4638 coarse-grained water for MARTINI 2.2P and 2.3P). For each force field, the bilayer was built and solvated using insane³⁹ and equilibrated using the gromit tool.⁵² For each window, we first carried out 5 ns of equilibration with a time step of 10 fs. During the equilibration, the side-chain analogue was pulled to the expected distance from the center of the bilayer. We carried out the production for 1 μ s per window with a time step of 20 fs for a total sampling of 41 μ s per side chain and for each force field. The pressure was coupled to 1 bar with a semi-isotropic Berendsen barostat, and

the temperature was coupled to 300 K using the Langevin thermostat. We used PME to treat the electrostatics beyond the cutoff.

3. RESULTS AND DISCUSSION

3.1. BtPI-PLC Does Not Bind to PC Bilayers When Simulated with MARTINI 2.2P. We first carry out membrane-binding simulations of BtPI-PLC. This protein binds to PC-rich membranes by engaging several tyrosine residues (Y88, Y246, Y251, Y204) in cation- π interactions with choline groups. Two tryptophan residues (W47, W242) insert below the phosphate plane and do not engage in cation- π interactions.²⁵ To test whether or not the MARTINI model can capture the known binding mode, we place the protein away from a pure DMPC membrane in its membrane binding orientation and run five simulations differing from each other by the initial protein-membrane distance (Figure 1A). Ideally, all simulations should converge to the experimentally known membrane-bound orientation (Figure 1B).

Out of these five simulations, none leads to a lasting binding event that involves the experimentally determined binding site. This is shown by the depths of anchoring per amino acid in each of the five simulations (Figure 2A). The protein comes in contact shortly with the membrane either in its correct orientation or with other sides facing the lipids (Figure S1, bottom panel). One of the simulations (sim 3 in Figure 2A) actually leads to the protein binding to the membrane in a wrong orientation in which it remains trapped. The depth of anchoring per residue (magenta line on Figure 2A) confirms that the amino acids close to the membrane in simulation 3 do not correspond to the binding site observed in all-atom simulations (data from Grauffel et al.²¹).

To rule out the possibility that the lack of binding is due to too limited sampling, we perform a membrane detachment test. We manually anchor the protein at the bilayer in the correct depth and orientation and run multiple simulations (Figure 1B). We want to check if the protein stays bound or detaches in relatively short simulations (500 ns). In all five simulations, the protein detaches from the membrane and the residence time varies from 50 to 350 ns (Figure S2). In one simulation (sim 2), the protein reattaches to the membrane, however, in a wrong orientation (Figure S3) similar to that observed in the membrane binding simulation (sim 3 in Figure 2A).

Together, these simulations show that MARTINI 2.2P needs further improvements to faithfully model interfacial membrane binding of proteins where aromatic amino acids are engaged in cation- π interactions. The further improvement of MARTINI 2.2P is discussed in the following sections.

3.2. Modification of MARTINI 2.2P for Cation- π Interactions: MARTINI 2.3P. For MARTINI to capture the binding of BtPI-PLC to a membrane, we modified the interaction matrix between bead types used in aromatic amino acids (P₁, C₄, and C₅) and the Q₀ bead, which is used to represent the choline headgroup of PC lipids. We gradually increased the interactions, testing several modifications (Table S1). The best one is coined "MARTINI 2.3P" and discussed henceforth. Briefly, the procedure for obtaining the modified interaction matrix was as follows:

1. Interactions were increased between each pair of beads, namely, Q₀ and each of P₁, C₄, and C₅. For example,

changes for Q₀-P₁ bead from level II to level I, changes for Q₀-C₅ bead from level IV to level III, and changes for Q₀-C₄ bead from level V to level IV, make one combination. All combinations tested are given in Supporting Information (Table S1).

2. For each combination, we performed membrane binding (Figure 1A) and membrane detachment (Figure 1B) simulations of the peripheral protein (BtPI-PLC in this case).
3. Membrane penetration depths are calculated for each amino acid of BtPI-PLC after the successful binding events and compared to the corresponding all-atom profile of the same protein to determine the final interaction matrix.

The changes in the interaction matrix that performed the best and current values are provided in Table 2.

Table 2. Reduced MARTINI 2.3P vs MARTINI 2.2P Interaction Matrices^a

	P ₁	C ₅	C ₄
Q ₀	I (II)	III (IV)	III (V)

^aMARTINI 2.3P values are in bold fonts; MARTINI 2.2P values are in parentheses. Level of interaction represents the Lennard-Jones (LJ) potential well depth (ϵ): I, $\epsilon = 5.0$ kJ/mol; II, $\epsilon = 4.5$ kJ/mol; III, $\epsilon = 4.0$ kJ/mol; IV, $\epsilon = 3.5$ kJ/mol; V, $\epsilon = 3.1$ kJ/mol. The LJ parameter σ is set to 0.47 nm for these interaction levels.

3.3 BtPI-PLC Does Bind Spontaneously to PC Bilayers When Simulated with MARTINI 2.3P. We perform similar binding simulations with "MARTINI 2.3P" as we did with "MARTINI 2.2P". In addition, we perform binding simulations starting from random starting protein orientation (Figure 1C).

The five simulations starting from the known binding orientation lead to BtPI-PLC binding the DMPC membrane in the same orientation (Figure 2B). Unlike with MARTINI 2.2P, the protein finds the membrane and converges to the right binding mode irrespective of the initial protein-membrane distance. The profiles of depth of anchoring per residue compare well to the profile from all-atom simulations.²¹ An analysis of the minimum protein-membrane distance and tilt angle for simulation 2 shows that the protein approaches the membrane and slightly reorients itself before binding within 100 ns (Figure S4). The protein remains stably bound until the end of the simulation at 500 ns. Other simulations show similar profiles. We determine the equilibrium tilt angle of the bound protein from the distribution of tilt angles along the simulations trajectory after binding event. All simulations show peaks around 10–15° (Figure S5) except for simulation 3 where we observe two equally probable peaks at around 15 and 45°. The protein in this case adopts (switches multiple times between) two conformations. This might be due to the smoother energy landscape of MARTINI CG force field or the fact that the CG force field allows improved sampling.

We next perform binding simulations starting from randomized orientations (Figure 1C), which is a more stringent test of the new parameters. In all but one simulation (simulation 5), the protein binds the membrane in the correct binding orientation (Figure 2C). The outcome of simulation 5 is discussed in the Section 3.6. The equilibrium tilt angle is equal to 10–15°, as observed for previous simulations (Figure S6).

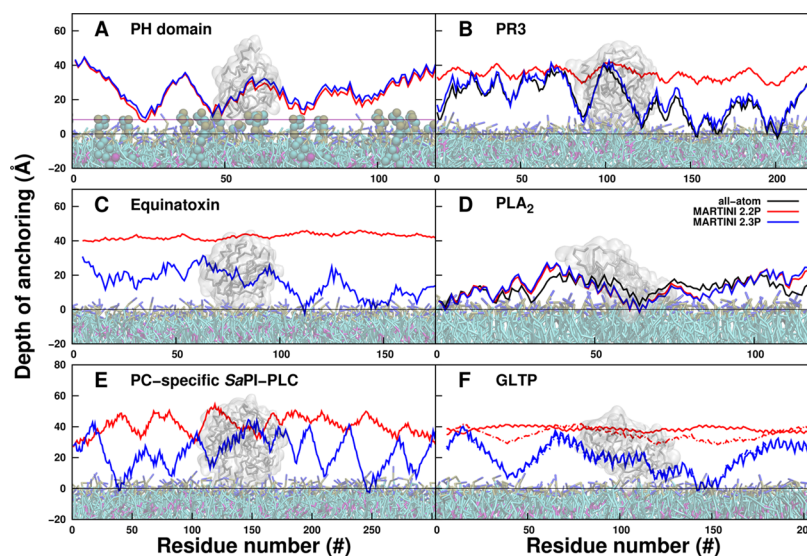


Figure 3. Depth of anchoring (per residue) beyond the phosphate plane of the membrane for different proteins in the dataset using MARTINI 2.2P and MARTINI 2.3P; calculated from the simulation trajectories. (A) PH domain, (B) proteinase 3, (C) equinatoxin, (D) phospholipase A₂, (E) PC-specific SaPI-PLC, and (F) glycolipid transfer protein. The PDB IDs are provided for each protein in Table 1 and Section 3.4.1. The membrane bound structures for each protein are provided in the corresponding panels and represented as in Figure 2D (except for PIP lipids which are represented with VDW spheres). The dash lines represent independent additional simulations. The reference profile is obtained for PR3 from all-atom simulation by Schillinger et al.⁶⁰ and for PLA₂ from all-atom simulation by Waheed et al.⁶¹ Phosphate plane is represented by a horizontal black line ($y = 0$) for all cases. As the localization of PH domain is close to the PI rings rather than the phosphate plane, PIP_n plane (horizontal magenta line) is also used for better description of the localization in this case. The positive control remains unaltered (A). MARTINI 2.2P does not manage to localize other proteins except PLA₂. On the other hand, MARTINI 2.3P manages to demonstrate correct binding orientation and localization of these proteins including identifying the key residues involved in membrane binding.

Overall, simulations with MARTINI 2.3P capture the membrane binding mode from all-atom simulations (Figure 2D), which is also in agreement with experimental data. The modified parameters thus capture the binding of a protein where not only cation- π interactions (by tyrosine) play an important role in membrane binding but also the tryptophan insertion is critical.

3.4. Evaluation of the Performance of MARTINI 2.3P for Additional Peripheral Membrane Proteins. To test how MARTINI 2.3P performs for peripheral proteins other than BtPI-PLC, we selected five proteins that are known to use aromatic amino acids to bind to PC-rich membranes and two control proteins: one that does not bind to PC-rich bilayers (WT SaPI-PLC) and one that binds but without involving aromatic amino acids (PLC- δ 1 PH domain). We performed membrane-binding tests on each of them and report the distance for the membrane insertion of each amino acid. Information about the seven proteins is given below, and information about the simulations is provided in Table 1 (Section 2).

3.4.1. Selected Proteins. **3.4.1.1. PLC- δ 1 PH Domain (PH Domain, PDB ID 1MAI).** PH domains are well known membrane targeting domains whose membrane binding is thought to be driven mostly by nonspecific electrostatic interactions.^{19,53} Both all-atom and CG MD simulations using MARTINI have been used to characterize the membrane binding mechanism of the PH domain of phospholipase C- δ 1.^{12–14,33,34,54} Relying on this, we chose it as a control, i.e., the new interaction matrix should not affect its binding to PIP_n containing PC-rich bilayers compared with MARTINI 2.2P.^{12,14,33,34}

3.4.1.2. Proteinase 3 (PR3, PDB ID 1FUJ). This neutrophil serine protease is a target for the treatment of chronic

inflammation.⁵⁵ PR3 has been reported to be present on the surface of neutrophils,⁵⁶ and its membrane binding site was identified using both experiments and molecular simulations.^{57–60} Notably, we highlighted the role of three phenylalanines and one tryptophan in the binding of PR3 to zwitterionic bilayers composed of POPC lipids.⁶⁰ We found in atomistic simulations that F166, F224, and W218 engage in cation- π interactions with PC lipids.⁶¹

3.4.1.3. Actinia equina Equinatoxin II (Equinatoxin, PDB ID 1IAZ). This is a pore-forming toxin from sea anemone. The monomers bind to the membrane prior to pore formation by oligomerization, and earlier experimental work highlighted the role of an “exposed aromatic cluster” in membrane attachment.⁶² A study combining NMR and MD provided further details on the critical residues involved in protein-lipid interactions with PC micelles, among which were W116, Y137, and Y138.²²

3.4.1.4. Naja naja atra Phospholipase A₂ (PLA₂, PDB ID 1POA). PLA₂ has been shown to use several aromatic amino acids for binding on zwitterionic membranes:^{63,64} two tyrosines (Y3, Y110), three tryptophans (W18, W19, W61), and one phenylalanine (F64),⁶⁵ of which W61 and Y110 are likely to engage in cation- π interactions with choline groups.⁶¹

3.4.1.5. Staphylococcus aureus Phosphatidylinositol-Specific Phospholipase C (SaPI-PLC); WT (WT SaPI-PLC, PDB ID 4F2T) and N254Y, H258Y Mutant (PC-Specific SaPI-PLC, PDB ID 4I8Y). WT SaPI-PLC shows virtually no affinity for PC lipids;⁶⁵ therefore, we used it as a negative control protein. Simulations with either version of MARTINI should not lead to membrane binding. We also used an engineered form that is PC-specific. Cheng et al. introduced two tyrosines (N254Y, H258Y) to mimic the cation- π box observed in the *Bacillus* PI-PLC.⁶⁵ X-ray crystallography of the engineered

Table 3. Properties of Lipid Bilayers Containing DLiPC Only, DLiPC/CHOL, or DPPC/DLiPC/CHOL Simulated with MARTINI 2.2P and MARTINI 2.3P

	DLiPC		DLiPC/CHOL		DLiPC/CHOL	
	v2.2P	v2.3P	v2.2P	v2.3P	v2.2P	v2.3P
average APL (nm ²)	0.784 ± 0.001	0.785 ± 0.001	0.806 ± 0.001	0.806 ± 0.001	0.743 ± 0.001	0.743 ± 0.001
average area compressibility (mN/m)	197 ± 5	205 ± 5	211 ± 19	231 ± 14	224 ± 27	240 ± 17
average tail order DLiPC	0.206 ± 0.001	0.201 ± 0.001	0.219 ± 0.002	0.215 ± 0.002	0.231 ± 0.002	0.226 ± 0.002
average tail order DPPC					0.574 ± 0.003	0.580 ± 0.003
average bilayer thickness (nm)	3.468 ± 0.001	3.453 ± 0.001	2.778 ± 0.003	2.791 ± 0.002	4.091 ± 0.003	4.086 ± 0.001
CHOL flip-flop rate (10 ⁶ s ⁻¹)			59 ± 3	57 ± 3	9.0 ± 0.4	8.3 ± 0.3

SaPI-PLC with choline or 1,2-dibutyl-*sn*-glycero-3-phosphocholine (diC₄PC) revealed two discrete PC binding sites. The first one contains four tyrosines: Y211, Y212, N254Y, H258Y. The second site contains two tyrosines and one tryptophan: H258Y, Y290, W287. In addition, W45 is important for membrane binding.

3.4.1.6. Bovine Glycolipid Transfer Protein (GLTP, PDB ID 1WBE).⁶⁶ Three tryptophans (W85, W96, W142) in the speculated membrane binding site are thought to be the primary contributors of membrane binding.^{67,68} Later biophysical experiments using fluorescence spectroscopy confirmed that W142 along with nearby residues is the primary contributor to membrane affinity.⁶⁹

3.4.2. Membrane-Binding Test. Figure 3 shows, for each of the proteins above, the depth of anchoring of their amino acids and helps identify amino acids located close to the lipids. In terms of membrane binding, the performance of MARTINI 2.3P is superior to MARTINI 2.2P. For the control protein PH domain (Figure 3A) and for PLA₂ (Figure 3D), where the binding events were already in the correct orientation with MARTINI 2.2P, the 2.3P parameter set does not bring any further improvements with respect to the all-atom reference simulations. We discuss the case of PLA₂ later in this section. Expectedly, WT SaPI-PLC, which serves as a negative control, did not bind to the bilayer in any of the two simulations with MARTINI 2.3P (data not shown).

The MARTINI 2.2P model fails to localize the other four proteins at the membrane surface (Figure 3B,C,E,F) while lasting binding events are observed with MARTINI 2.3P, which also identifies residues critical for membrane binding. For PR3, the membrane-penetrating segments are identical to those observed with all-atom MD simulations, notably the insertion of the critical aromatic amino acids (Figure 3B). For equinatoxin, the following residues are identified: R144, W116, S114, W112, Y113, Y138, Y137 (Figure 3C), in agreement with the work of Weber et al.²² For the PC-specific SaPI-PLC mutant, the identified membrane binding site includes the aromatic amino acids reported by Cheng et al.⁶⁵ and the putative helix B region involved in membrane binding of bacterial PI-PLCs²⁵ (Figure 3E). Both simulations of GLTP converge to the same membrane binding orientation (Figure 3F). Note that one of the simulations is initiated with a random orientation and one in the membrane binding orientation (Table 1). Interestingly, W142 and adjacent isoleucines (I143, I147) localize close to the phosphate plane or penetrate as suggested by previous works.⁶⁹ We also observe that the localization of the protein on the membrane surface is shallow, consistent with experimental data.

Unlike the other proteins tested, the simulations of PLA₂ lead to similar membrane-bound depths and orientations with both the MARTINI 2.2P and MARTINI 2.3P models (Figure

3D). When compared with all-atom data, we find that the main membrane binding region of the protein (containing W61, F64) penetrates deeper than in all-atom simulation data⁶¹ (black line in Figure 3D). This deeper penetration is also true for another segment containing two consecutive Asn residues located along with several Gly, Ala, and Val (-⁸⁰G-G-N-N-A-C-A-A-A-V⁸⁹-). This difference might originate from two factors: (i) the protein cannot make subtle structural adjustments in the CG simulations as it can in all-atom simulations; (ii) the Asn and Gln hydrophobicity in the MARTINI model leads to a deeper insertion of the 80–89 segment than it should. The latter is further discussed in the Section 3.6.

All in all, MARTINI 2.3P leads to significant improvements in terms of peripheral membrane protein localization and identification of critical membrane binding segments and agrees well with all-atom simulations and experimental data for the cases tested here.

3.5. Control Simulations. To ensure that our modifications of the interaction matrix do not introduce biases in simulations of other systems, we performed a set of control simulations of lipid bilayers, a transmembrane protein, and amino acid translocation through lipid bilayers. Each system was simulated with MARTINI 2.2P and MARTINI 2.3P using the same simulation parameters.

3.5.1. Membrane Properties Remain Unaltered. The doubly unsaturated tails of DLiPC are modeled using two C₄ beads per lipid tail and a Q₀ bead for the choline group. We simulated bilayers containing DLiPC to ensure that our modification of the C₄–Q₀ interaction (Table 2) does not affect the properties of DLiPC-containing bilayers. In addition, we looked at mixtures of DLiPC and cholesterol (CHOL) and a DPPC/DLiPC/CHOL biphasic mixture, as cholesterol is modeled with P₁ bead. Table 3 lists for each bilayer the average area per lipid (APL), area compressibility, tail order parameter, diffusion coefficient, and bilayer thickness (measured between the phosphate groups).

The calculated properties are almost unaffected by the applied modifications. For example, the average tail order of the DLiPC bilayer is slightly reduced with MARTINI 2.3P compared with MARTINI 2.2P and it is accompanied by a slight decrease of the bilayer thickness. The APL and the area compressibility are the same within the error estimates. The same is true for the CHOL flip-flop rates. The lateral density profiles as well as the relative number of neighboring lipids in the DPPC/DLiPC/CHOL bilayer are also virtually unaffected by the applied modifications (see Figures S7, S8, and Table S2 in the Supporting Information). Overall, the differences in the bilayer properties between the two MARTINI versions are marginal and well within the accuracy of the force field.

3.5.2. Effects on Transmembrane Proteins are Negligible. It is important to check a possible effect of our force field

modification on interactions between aromatic residues of transmembrane proteins and lipids. In particular, we need to ensure that choline heads do not artificially penetrate below the phosphate plane to interact with aromatic amino acids located in the transmembrane region. We chose bovine rhodopsin (PDB ID: 1U19) for this purpose. It contains 54 aromatic amino acids. According to OPM,⁴⁰ 34 of these aromatic amino acids have their $C\alpha$ position located in the hydrophobic region of the bilayer (Figure S9).

We performed 500 ns long simulations of a rhodopsin monomer embedded in a POPC bilayer, using both MARTINI 2.2P and MARTINI 2.3P. We evaluate the integrity of the lipid bilayer through the calculation of four properties: (i) tilt angle of rhodopsin with respect to the bilayer normal, (ii) average number of POPC–rhodopsin contacts, (iii) bead density profile for protein, phosphate, and choline groups along the bilayer normal, and (iv) POPC head occupancy around rhodopsin.

The results, presented in Table 4, show that rhodopsin–POPC interactions remain mostly unaffected by the changes

Table 4. Average Rhodopsin Tilt Angle and Average Number of POPC–Rhodopsin Contacts Calculated for Simulations with MARTINI 2.2P and MARTINI 2.3P

MARTINI version		v2.2P	v2.3P	percentage difference (%)
tilt angle (deg)		16.1 ± 0.4	15.6 ± 0.7	3.2
type of contacts	head-protein	319 ± 8	334 ± 6	4.6
	tail-protein	736 ± 8	741 ± 4	0.7
	head-aromatic residues	63 ± 2	68 ± 1	7.6
	tail-aromatic residues	331 ± 4	335 ± 2	1.2

introduced in MARTINI 2.3P, relative to MARTINI 2.2P. We observe a small increase in the number of contacts between lipid heads and aromatic residues in simulations run with version 2.3P. The average tilt angle of rhodopsin is slightly reduced, which indicates that rhodopsin orientation in the POPC bilayer is closer to the tilt angles values obtained in MD simulations with the standard nonpolarizable MARTINI (around 10°)⁷⁰ than to the values obtained with 2.2P. These small differences do not impact the overall bilayer deformation around the protein, as shown in Figure S10. Partial density profiles obtained from both MARTINI 2.2P and MARTINI 2.3P largely overlap for the protein, water, phosphates, and cholines. Small changes are only noticeable in the occupancy densities around rhodopsin, which shows slightly more bilayer deformation in MARTINI 2.3P, mainly around residues in the head–water interface. The overall membrane deformation in both versions of polarizable MARTINI is in good agreement with the bilayer deformation observed in atomistic MD simulations.⁷¹

3.5.3. Membrane Translocation PMF of Aromatic Amino Acids. As the modification in MARTINI 2.3P involves interactions between the PC lipid headgroups and the aromatic side chains, we need to evaluate the effect of the change in parameters on the membrane translocation PMF of these three amino acids. We choose a DOPC bilayer (Figure S11) for that purpose, and we compare the PMF profiles obtained with both force fields⁶ and to the atomistic PMF profiles from MacCallum et al.⁷²

The trend is very similar for all aromatics when we compare 2.3P to 2.2P. With 2.3P, we observe a slight decrease from the PMF minimum and up to the phosphate plane region (1–2 nm) for all profiles. A larger difference is observed right above the phosphate plane (2–2.2 nm), especially for Tyr and Trp. The PMF profiles are almost overlapping in the membrane core region (0–1 nm).

The barrier just above the phosphate plane is lower with 2.3P than with 2.2P for both Tyr and Trp. 2.3P is thus closer to the atomistic profile in this region. The 2–3 kJ/mol barrier observed for Phe (atomistic) in the same region is reduced in the PMF profile obtained using MARTINI 2.3P. The meaning and relevance of this low barrier in the headgroup region is somewhat unclear. It is not present in the PMF profile of Phe translocation obtained using the highly mobile membrane mimetic (HMMM) models by Pogorelov et al.⁷³ We also observe a large energy difference (around 10 kJ/mol) between Tyr atomistic PMF profile and coarse grain PMF profiles in the region close to the bilayer center (0–0.5 nm). However, this is true for both 2.3P and 2.2P so it is not caused by the modifications we introduced. Furthermore, it should be noted that the atomistic PMF profile has a large error (more than 5 kJ/mol) in this particular region. Further investigation is needed for clarification of this difference; as such difference is not present in other regions/profiles.

3.6. Limitations of the Proposed Model. In this section, we discuss some limitations of the application of the MARTINI model, and of our modifications, to peripheral proteins.

First, it is worth being reminded that the use of the elastic network to keep the protein tertiary structure preserved during CG simulations precludes the study of proteins whose binding to membranes require structural rearrangements, even if they are subtle.

The membrane translocation PMF calculated by de Jong et al. shows that all-atom PMFs for both Asn and Gln have a low energy barrier just above the phosphates⁶ while the MARTINI 2.2P PMFs show no such barrier but decrease from bulk water to the bilayer hydrophobic core. In other words, Asn and Gln residues tend to localize deeper than expected with MARTINI 2.2P. For a peripheral protein, this means that a segment containing multiple Asn and/or Gln residues along with other hydrophobic residues will have a tendency to insert deeper than it should in the membrane interface. We observe that behavior for the PLA₂ localization (Figure 3D). In addition, such a segment can compete with the actual membrane binding segment and lead to the wrong membrane-bound orientation, as we observed in one of the simulations of BtPI-PLC (sim 5 in Figure 2C). Further, there is virtually no barrier for the insertion of histidine residues in the membrane core with MARTINI 2.2P. As His residue shares atom types with other aromatic amino acids, our modification renders their membrane insertion more favorable (Figure S12). This may affect peripheral protein binding in the same way as described above for Asn and Gln residues.

As a final remark, it is important to note that the correction proposed here is only applicable to the polarizable version of MARTINI.⁴¹ In the standard nonpolarizable MARTINI 2.2, all interactions involving charged Q-beads and neutral beads (P, C and N types) are reduced by one level in relation to the polarizable MARTINI 2.2P model. As consequence, a shift of two levels would be necessary to get a similar effect as we described here. This modification is too drastic for the

standard model, as Q_0 interactions with P1, C5, and C4 would be completely out of the expected interaction trends in relation to other beads. A full reparametrization of Q-beads would be required. This will be performed as part of the forthcoming MARTINI 3.0 version.

4. CONCLUSIONS AND FUTURE PERSPECTIVES

In this work, we present a modified version of the polarizable MARTINI 2.2P model where the interaction matrix is adjusted to better account for interactions between aromatic amino acids and PC lipids. This modification implicitly accounts for cation– π interactions. It also provides a better description of interfacial aromatic amino acids in the context of peripheral membrane binding, as demonstrated by the results of our systematic tests, including both positive and negative controls. MARTINI 2.3P leads to membrane binding orientations similar to atomic resolutions and identification of experimentally determined membrane binding residues. The curated dataset of peripheral proteins that was used for this work will be useful for other force fields developments, including the standard nonpolarizable version of MARTINI 3.0. We verified that the new interaction matrix did not introduce biases in simulations of other systems. Hence, MARTINI 2.3P is a significant improvement over its predecessor MARTINI 2.2P, and is recommended for any study involving peripheral binding of membrane peptides and proteins as well as other systems where cation– π interactions could potentially be crucial.

■ ASSOCIATED CONTENT

SI Supporting Information

The Supporting Information is available free of charge at <https://pubs.acs.org/doi/10.1021/acs.jctc.9b01194>.

Tested interaction levels (Table S1), relative number of neighboring lipid in ternary bilayer systems (Table S2); analysis on peripheral protein (*BtPI-PLC*) using MARTINI 2.2P and MARTINI 2.3P: minimum protein–membrane distances and tilt angles (Figures S1–S4), tilt angle distributions (Figures S5 and S6); figures and analyses on bilayer systems: top and side view of the systems (Figure S7), density profiles (Figure S8); PDB structure and analysis on transmembrane protein: PDB structure with membrane localization (Figure S9), density profiles (Figure S10); membrane translocation PMF of amino acids: aromatic amino acids (Figure S11), histidine (Figure S12) (PDF)

■ AUTHOR INFORMATION

Corresponding Authors

Hanif M. Khan – Department of Biological Sciences and Computational Biology Unit, Department of Informatics, University of Bergen, N-5020 Bergen, Norway; orcid.org/0000-0001-5301-7234; Email: hanif.khan@uib.no

Nathalie Reuter – Department of Chemistry and Computational Biology Unit, Department of Informatics, University of Bergen, N-5020 Bergen, Norway; orcid.org/0000-0002-3649-7675; Email: nathalie.reuter@uib.no

Authors

Paulo C. T. Souza – Groningen Biomolecular Sciences and Biotechnology Institute and Zernike Institute for Advanced

Materials, University of Groningen, 9747 AG Groningen, Netherlands; orcid.org/0000-0003-0660-1301

Sebastian Thallmair – Groningen Biomolecular Sciences and Biotechnology Institute and Zernike Institute for Advanced Materials, University of Groningen, 9747 AG Groningen, Netherlands; orcid.org/0000-0002-3396-5840

Jonathan Barnoud – Groningen Biomolecular Sciences and Biotechnology Institute and Zernike Institute for Advanced Materials, University of Groningen, 9747 AG Groningen, Netherlands

Alex H. de Vries – Groningen Biomolecular Sciences and Biotechnology Institute and Zernike Institute for Advanced Materials, University of Groningen, 9747 AG Groningen, Netherlands

Siewert J. Marrink – Groningen Biomolecular Sciences and Biotechnology Institute and Zernike Institute for Advanced Materials, University of Groningen, 9747 AG Groningen, Netherlands; orcid.org/0000-0001-8423-5277

Complete contact information is available at:

<https://pubs.acs.org/10.1021/acs.jctc.9b01194>

Author Contributions

H.M.K. and N.R. conceived and initiated the project. H.M.K. and P.C.T.S. designed the modifications in the interaction matrix. H.M.K. performed all simulations involving peripheral membrane proteins. P.C.T.S., S.T. and J.B. performed all control simulations. All authors analyzed the results. H.M.K. wrote the manuscript with contributions from all authors. A.H.d.V., S.J.M., and N.R. supervised the work.

Notes

The authors declare no competing financial interest.

■ ACKNOWLEDGMENTS

The computations were performed on resources provided by UNINETT Sigma2—the National Infrastructure for High Performance Computing and Data Storage in Norway (project number 4700k) and on the Peregrine high-performance computing cluster of the University of Groningen. We would like to acknowledge the Center for Information Technology of the University of Groningen for their support and for providing access to the Peregrine high-performance computing cluster. N.R. and H.M.K. received funding from the Norwegian Research Council (FRIMEDBIO #251247 and #288008). S.J.M. received funding from the European Research Council (ERC) through an ERC Advanced grant “COMP-MICR-CROW-MEM”. S.T. acknowledges the support from the European Commission via a Marie Skłodowska-Curie Actions individual fellowship (MicroMod-PSII, grant agreement 748895). The authors would like to thank Drew Bennett for kindly providing the original data sets for the membrane translocation PMF of amino acids.

■ ABBREVIATIONS

MD, molecular dynamics; CG, coarse grain; *BtPI-PLC*, *Bacillus thuringiensis* phosphatidylinositol-specific phospholipase C; PR3, proteinase 3; *SaPI-PLC*, *Staphylococcus aureus* phosphatidylinositol-specific phospholipase C; GLTP, glycolipid transfer proteins

■ REFERENCES

(1) Ingólfsson, H. I.; Lopez, C. A.; Uusitalo, J. J.; de Jong, D. H.; Gopal, S. M.; Periole, X.; Marrink, S. J. the Power of Coarse Graining

in Biomolecular Simulations. *Wiley Interdiscip. Rev.: Comput. Mol. Sci.* **2014**, *4*, 225–248.

(2) Marrink, S. J.; Tieleman, D. P. Perspective on the Martini Model. *Chem. Soc. Rev.* **2013**, *42*, 6801–6822.

(3) Marrink, S. J.; de Vries, A. H.; Mark, A. E. Coarse Grained Model for Semiquantitative Lipid Simulations. *J. Phys. Chem. B* **2004**, *108*, 750–760.

(4) Marrink, S. J.; Risselada, H. J.; Yefimov, S.; Tieleman, D. P.; de Vries, A. H. The MARTINI Force Field: Coarse Grained Model for Biomolecular Simulations. *J. Phys. Chem. B* **2007**, *111*, 7812–7824.

(5) Monticelli, L.; Kandasamy, S. K.; Periole, X.; Larson, R. G.; Tieleman, D. P.; Marrink, S.-J. The MARTINI Coarse-Grained Force Field: Extension to Proteins. *J. Chem. Theory Comput.* **2008**, *4*, 819–834.

(6) de Jong, D. H.; Singh, G.; Bennett, W. F. D.; Arnarez, C.; Wassenaar, T. A.; Schäfer, L. V.; Periole, X.; Tieleman, D. P.; Marrink, S. J. Improved Parameters for the Martini Coarse-Grained Protein Force Field. *J. Chem. Theory Comput.* **2013**, *9*, 687–697.

(7) López, C. A.; Rzepiela, A. J.; de Vries, A. H.; Dijkhuizen, L.; Hünenberger, P. H.; Marrink, S. J. Martini Coarse-Grained Force Field: Extension to Carbohydrates. *J. Chem. Theory Comput.* **2009**, *5*, 3195–3210.

(8) Uusitalo, J. J.; Ingólfsson, H. I.; Akhshi, P.; Tieleman, D. P.; Marrink, S. J. Martini Coarse-Grained Force Field: Extension to DNA. *J. Chem. Theory Comput.* **2015**, *11*, 3932–3945.

(9) Uusitalo, J. J.; Ingólfsson, H. I.; Marrink, S. J.; Faustino, I. Martini Coarse-Grained Force Field: Extension to RNA. *Biophys. J.* **2017**, *113*, 246–256.

(10) Corradi, V.; Sengupta, B. I.; Mesa-Gallosio, H.; Abdizadeh, H.; Noskov, S. Y.; Marrink, S. J.; Tieleman, D. P. Emerging Diversity in Lipid–Protein Interactions. *Chem. Rev.* **2019**, *119*, 5775–5848.

(11) Marrink, S. J.; Corradi, V.; Souza, P. C. T.; Ingólfsson, H. I.; Tieleman, D. P.; Sansom, M. S. P. Computational Modeling of Realistic Cell Membranes. *Chem. Rev.* **2019**, *119*, 6184–6226.

(12) Yamamoto, E.; Kalli, A. C.; Yasuoka, K.; Sansom, M. S. P. Interactions of Pleckstrin Homology Domains with Membranes: Adding Back the Bilayer via High-Throughput Molecular Dynamics. *Structure* **2016**, *24*, 1421–1431.

(13) Lumb, C. N.; Sansom, M. S. P. Finding a Needle in a Haystack: The Role of Electrostatics in Target Lipid Recognition by PH Domains. *PLoS Comput. Biol.* **2012**, *8*, e1002617.

(14) Naughton, F. B.; Kalli, A. C.; Sansom, M. S. P. Modes of Interaction of Pleckstrin Homology Domains with Membranes: Toward a Computational Biochemistry of Membrane Recognition. *J. Mol. Biol.* **2018**, *430*, 372–388.

(15) Sun, F.; Schroer, C. F. E.; Xu, L.; Yin, H.; Marrink, S. J.; Luo, S.-Z. Molecular Dynamics of the Association of L-Selectin and FERM Regulated by PIP2. *Biophys. J.* **2018**, *114*, 1858–1868.

(16) Sengupta, D. Cholesterol Modulates the Structure, Binding Modes, and Energetics of Caveolin–Membrane Interactions. *J. Phys. Chem. B* **2012**, *116*, 14556–14564.

(17) Hofbauer, H. F.; Gecht, M.; Fischer, S. C.; Seybert, A.; Frangakis, A. S.; Stelzer, E. H. K.; Covino, R.; Hummer, G.; Ernst, R. The molecular recognition of phosphatidic acid by an amphipathic helix in Opi1. *J. Cell Biol.* **2018**, *217*, 3109–3126.

(18) Johnson, J. E.; Cornell, R. B. Amphitropic proteins: regulation by reversible membrane interactions. *Mol. Membr. Biol.* **1999**, *16*, 217–235.

(19) Cho, W.; Stahelin, R. V. Membrane-Protein Interactions in Cell Signaling and Membrane Trafficking. *Annu. Rev. Biophys. Biomol. Struct.* **2005**, *34*, 119–151.

(20) Jacobs, R. E.; White, S. H. The nature of the hydrophobic binding of small peptides at the bilayer interface: implications for the insertion of transbilayer helices. *Biochemistry* **1989**, *28*, 3421–3437.

(21) Grauffel, C.; Yang, B.; He, T.; Roberts, M. F.; Gershenson, A.; Reuter, N. Cation- π Interactions As Lipid-Specific Anchors for Phosphatidylinositol-Specific Phospholipase C. *J. Am. Chem. Soc.* **2013**, *135*, 5740–5750.

(22) Weber, D. K.; Yao, S.; Rojko, N.; Anderlueh, G.; Lybrand, T. P.; Downton, M. T.; Wagner, J.; Separovic, F. Characterization of the Lipid-Binding Site of Equinatoxin II by NMR and Molecular Dynamics Simulation. *Biophys. J.* **2015**, *108*, 1987–1996.

(23) Goh, B. C.; Wu, H.; Rynkiewicz, M. J.; Schulten, K.; Seaton, B. A.; McCormack, F. X. Elucidation of Lipid Binding Sites on Lung Surfactant Protein A Using X-ray Crystallography, Mutagenesis, and Molecular Dynamics Simulations. *Biochemistry* **2016**, *55*, 3692–3701.

(24) Hirano, Y.; Gao, Y.-G.; Stephenson, D. J.; Vu, N. T.; Malinina, L.; Simanshu, D. K.; Chalfant, C. E.; Patel, D. J.; Brown, R. E. Structural basis of phosphatidylcholine recognition by the C2-domain of cytosolic phospholipase A₂ α . *eLife* **2019**, *8*, e44760.

(25) Roberts, M. F.; Khan, H. M.; Goldstein, R.; Reuter, N.; Gershenson, A. Search and Subvert: Minimalist Bacterial Phosphatidylinositol-Specific Phospholipase C Enzymes. *Chem. Rev.* **2018**, *118*, 8435–8473.

(26) Yang, B.; Pu, M.; Khan, H. M.; Friedman, L.; Reuter, N.; Roberts, M. F.; Gershenson, A. Quantifying Transient Interactions between Bacillus Phosphatidylinositol-Specific Phospholipase-C and Phosphatidylcholine-Rich Vesicles. *J. Am. Chem. Soc.* **2015**, *137*, 14–17.

(27) Khan, H. M.; He, T.; Fuglebakk, E.; Grauffel, C.; Yang, B.; Roberts, M. F.; Gershenson, A.; Reuter, N. A Role for Weak Electrostatic Interactions in Peripheral Membrane Protein Binding. *Biophys. J.* **2016**, *110*, 1367–1378.

(28) Petersen, F. N. R.; Jensen, M. Ø.; Nielsen, C. H. Interfacial Tryptophan Residues: A Role for the Cation- π Effect? *Biophys. J.* **2005**, *89*, 3985–3996.

(29) Khan, H. M.; Grauffel, C.; Broer, R.; MacKerell, A. D.; Havenith, R. W. A.; Reuter, N. Improving the Force Field Description of Tyrosine–Choline Cation- π Interactions: QM Investigation of Phenol–N(Me)₄⁺ Interactions. *J. Chem. Theory Comput.* **2016**, *12*, 5585–5595.

(30) Khan, H. M.; MacKerell, A. D.; Reuter, N. Cation- π Interactions between Methylated Ammonium Groups and Tryptophan in the CHARMM36 Additive Force Field. *J. Chem. Theory Comput.* **2019**, *15*, 7–12.

(31) Barrera, E. E.; Machado, M. R.; Pantano, S. Fat SIRAH: Coarse-Grained Phospholipids To Explore Membrane–Protein Dynamics. *J. Chem. Theory Comput.* **2019**, *15*, 5674–5688.

(32) Herzog, F. A.; Braun, L.; Schoen, I.; Vogel, V. Improved Side Chain Dynamics in MARTINI Simulations of Protein–Lipid Interfaces. *J. Chem. Theory Comput.* **2016**, *12*, 2446–2458.

(33) Buyan, A.; Kalli, A. C.; Sansom, M. S. P. Multiscale Simulations Suggest a Mechanism for the Association of the Dok7 PH Domain with PIP-Containing Membranes. *PLoS Comput. Biol.* **2016**, *12*, No. e1005028.

(34) Naughton, F. B.; Kalli, A. C.; Sansom, M. S. P. Association of Peripheral Membrane Proteins with Membranes: Free Energy of Binding of GRP1 PH Domain with Phosphatidylinositol Phosphate-Containing Model Bilayers. *J. Phys. Chem. Lett.* **2016**, *7*, 1219–1224.

(35) Thukral, L.; Sengupta, D.; Ramkumar, A.; Murthy, D.; Agrawal, N.; Gokhale; Rajesh, S. The Molecular Mechanism Underlying Recruitment and Insertion of Lipid-Anchored LC3 Protein into Membranes. *Biophys. J.* **2015**, *109*, 2067–2078.

(36) Atsmon-Raz, Y.; Tieleman, D. P. Parameterization of Palmitoylated Cysteine, Farnesylated Cysteine, Geranylgeranylated Cysteine, and Myristoylated Glycine for the Martini Force Field. *J. Phys. Chem. B* **2017**, *121*, 11132–11143.

(37) Shi, X.; Shao, C.; Zhang, X.; Zambonelli, C.; Redfield, A. G.; Head, J. F.; Seaton, B. A.; Roberts, M. F. Modulation of *Bacillus thuringiensis* Phosphatidylinositol-specific Phospholipase C Activity by Mutations in the Putative Dimerization Interface. *J. Biol. Chem.* **2009**, *284*, 15607–15618.

(38) Shao, C.; Shi, X.; Wehbi, H.; Zambonelli, C.; Head, J. F.; Seaton, B. A.; Roberts, M. F. Dimer Structure of an Interfacially Impaired Phosphatidylinositol-specific Phospholipase C. *J. Biol. Chem.* **2007**, *282*, 9228–9235.

- (39) Wassenaar, T. A.; Ingólfsson, H. I.; Böckmann, R. A.; Tieleman, D. P.; Marrink, S. J. Computational Lipidomics with Insane: A Versatile Tool for Generating Custom Membranes for Molecular Simulations. *J. Chem. Theory Comput.* **2015**, *11*, 2144–2155.
- (40) Lomize, M. A.; Lomize, A. L.; Pogozheva, I. D.; Mosberg, H. I. OPM: Orientations of Proteins in Membranes database. *Bioinformatics* **2006**, *22*, 623–625.
- (41) Yesylevskyy, S. O.; Schäfer, L. V.; Sengupta, D.; Marrink, S. J. Polarizable Water Model for the Coarse-Grained MARTINI Force Field. *PLoS Comput. Biol.* **2010**, *6*, e1000810.
- (42) Periole, X.; Cavalli, M.; Marrink, S.-J.; Ceruso, M. A. Combining an Elastic Network With a Coarse-Grained Molecular Force Field: Structure, Dynamics, and Intermolecular Recognition. *J. Chem. Theory Comput.* **2009**, *5*, 2531–2543.
- (43) Bussi, G.; Donadio, D.; Parrinello, M. Canonical Sampling through Velocity Rescaling. *J. Chem. Phys.* **2007**, *126*, 014101.
- (44) Parrinello, M.; Rahman, A. Polymorphic Transitions in Single Crystals: A New Molecular Dynamics Method. *J. Appl. Phys.* **1981**, *52*, 7182–7190.
- (45) Essmann, U.; Perera, L.; Berkowitz, M. L.; Darden, T.; Lee, H.; Pedersen, L. G. A Smooth Particle Mesh Ewald Method. *J. Chem. Phys.* **1995**, *103*, 8577–8593.
- (46) de Jong, D. H.; Baoukina, S.; Ingólfsson, H. I.; Marrink, S. J. Martini Straight: Boosting Performance Using a Shorter Cutoff and GPUs. *Comput. Phys. Commun.* **2016**, *199*, 1–7.
- (47) Van Der Spoel, D.; Lindahl, E.; Hess, B.; Groenhof, G.; Mark, A. E.; Berendsen, H. J. C. GROMACS: Fast, flexible, and Free. *J. Comput. Chem.* **2005**, *26*, 1701–1718.
- (48) Pronk, S.; Páll, S.; Schulz, R.; Larsson, P.; Bjelkmar, P.; Apostolov, R.; Shirts, M. R.; Smith, J. C.; Kasson, P. M.; van der Spoel, D.; Hess, B.; Lindahl, E. GROMACS 4.5: A High-Throughput and Highly Parallel Open Source Molecular Simulation Toolkit. *Bioinformatics* **2013**, *29*, 845–854.
- (49) Humphrey, W.; Dalke, A.; Schulten, K. VMD: Visual Molecular Dynamics. *J. Mol. Graphics* **1996**, *14*, 33–38.
- (50) Risselada, H. J.; Marrink, S. J. The Molecular Face of Lipid Rafts in Model Membranes. *Proc. Natl. Acad. Sci. U.S.A.* **2008**, *105*, 17367–17372.
- (51) Hub, J. S.; de Groot, B. L.; van der Spoel, D. g_wham—A Free Weighted Histogram Analysis Implementation Including Robust Error and Autocorrelation Estimates. *J. Chem. Theory Comput.* **2010**, *6*, 3713–3720.
- (52) <https://github.com/Tsjerk/gromit>.
- (53) Mulgrew-Nesbitt, A.; Diraviyam, K.; Wang, J.; Singh, S.; Murray, P.; Li, Z.; Rogers, L.; Mirkovic, N.; Murray, D. The Role of Electrostatics in Protein–Membrane Interactions. *Biochim. Biophys. Acta, Mol. Cell Biol. Lipids* **2006**, *1761*, 812–826.
- (54) Lai, C.-L.; Srivastava, A.; Pilling, C.; Chase, A. R.; Falke, J. J.; Voth, G. A. Molecular Mechanism of Membrane Binding of the GRP1 PH Domain. *J. Mol. Biol.* **2013**, *425*, 3073–3090.
- (55) Korkmaz, B.; Horwitz, M. S.; Jenne, D. E.; Gauthier, F. Neutrophil Elastase, Proteinase 3, and Cathepsin G as Therapeutic Targets in Human Diseases. *Pharmacol. Rev.* **2010**, *62*, 726–759.
- (56) Witko-Sarsat, V.; Cramer, E. M.; Hieblot, C.; Guichard, J.; Nusbaum, P.; Lopez, S.; Lesavre, P.; Halbwachs-Mecarelli, L. Presence of Proteinase 3 in Secretory Vesicles: Evidence of a Novel, Highly Mobilizable Intracellular Pool Distinct From Azurophil Granules. *Blood* **1999**, *94*, 2487–2496.
- (57) Goldmann, W. H.; Niles, J. L.; Arnaout, M. A. Interaction of Purified Human Proteinase 3 (Pr3) With Reconstituted Lipid Bilayers. *Eur. J. Biochem.* **1999**, *261*, 155–162.
- (58) Hajjar, E.; Mihajlovic, M.; Witko-Sarsat, V.; Lazaridis, T.; Reuter, N. Computational prediction of the binding site of proteinase 3 to the plasma membrane. *Proteins: Struct., Funct., Bioinf.* **2008**, *71*, 1655–1669.
- (59) Broemstrup, T.; Reuter, N. How does Proteinase 3 interact with lipid bilayers? *Phys. Chem. Chem. Phys.* **2010**, *12*, 7487–7496.
- (60) Schillinger, A.-S.; Grauffel, C.; Khan, H. M.; Halskau, Ø.; Reuter, N. Two Homologous Neutrophil Serine Proteases Bind to POPC Vesicles with Different Affinities: When Aromatic Amino Acids Matter. *Biochim. Biophys. Acta, Biomembr.* **2014**, *1838*, 3191–3202.
- (61) Waheed, Q.; Khan, H. M.; He, T.; Roberts, M.; Gershenson, A.; Reuter, N. Interfacial Aromatics Mediating Cation– π Interactions with Choline-Containing Lipids Can Contribute as Much to Peripheral Protein Affinity for Membranes as Aromatics Inserted below the Phosphates. *J. Phys. Chem. Lett.* **2019**, 3972–3977.
- (62) Hong, Q.; Gutiérrez-Aguirre, I.; Barlič, A.; Malovrh, P.; Kristan, K.; Podlesek, Z.; Maček, P.; Turk, D.; González-Mañas, J. M.; Lakey, J. H.; Anderlüh, G. Two-step Membrane Binding by Equinatoxin II, a Pore-forming Toxin from the Sea Anemone, Involves an Exposed Aromatic Cluster and a Flexible Helix. *J. Biol. Chem.* **2002**, *277*, 41916–41924.
- (63) Sumandea, M.; Das, S.; Sumandea, C.; Cho, W. Roles of Aromatic Residues in High Interfacial Activity of *Naja naja atra* Phospholipase A2. *Biochemistry* **1999**, *38*, 16290–16297.
- (64) Stahelin, R. V.; Cho, W. Differential Roles of Ionic, Aliphatic, and Aromatic Residues in Membrane–Protein Interactions: A Surface Plasmon Resonance Study on Phospholipases A2. *Biochemistry* **2001**, *40*, 4672–4678.
- (65) Cheng, J.; Goldstein, R.; Gershenson, A.; Stec, B.; Roberts, M. F. The Cation– π Box Is a Specific Phosphatidylcholine Membrane Targeting Motif. *J. Biol. Chem.* **2013**, *288*, 14863–14873.
- (66) Airene, T. T.; Kidron, H.; Nymalm, Y.; Nylund, M.; West, G.; Mattjus, P.; Salminen, T. A. Structural Evidence for Adaptive Ligand Binding of Glycolipid Transfer Protein. *J. Mol. Biol.* **2006**, *355*, 224–236.
- (67) Brown, R. E.; Mattjus, P. Glycolipid Transfer Proteins. *Biochim. Biophys. Acta, Mol. Cell Biol. Lipids* **2007**, *1771*, 746–760.
- (68) Mattjus, P. Glycolipid Transfer Proteins and Membrane Interaction. *Biochim. Biophys. Acta, Biomembr.* **2009**, *1788*, 267–272.
- (69) Kamlekar, R. K.; Gao, Y.; Kenoth, R.; Molotkovsky, J. G.; Prendergast, F. G.; Malinina, L.; Patel, D. J.; Wessels, W. S.; Venyaminov, S. Y.; Brown, R. E. Human GLTP: Three Distinct Functions for the Three Tryptophans in a Novel Peripheral Amphitropic Fold. *Biophys. J.* **2010**, *99*, 2626–2635.
- (70) Periole, X.; Huber, T.; Marrink, S.-J.; Sakmar, T. P. G Protein-Coupled Receptors Self-Assemble in Dynamics Simulations of Model Bilayers. *J. Am. Chem. Soc.* **2007**, *129*, 10126–10132.
- (71) Periole, X. Interplay of G Protein-Coupled Receptors with the Membrane: Insights from Supra-Atomic Coarse Grain Molecular Dynamics Simulations. *Chem. Rev.* **2017**, *117*, 156–185.
- (72) MacCallum, J. L.; Bennett, W. F. D.; Tieleman, D. P. Distribution of Amino Acids in a Lipid Bilayer from Computer Simulations. *Biophys. J.* **2008**, *94*, 3393–3404.
- (73) Pogorelov, T. V.; Vermaas, J. V.; Arcario, M. J.; Tajkhorshid, E. Partitioning of Amino Acids into a Model Membrane: Capturing the Interface. *J. Phys. Chem. B* **2014**, *118*, 1481–1492.